ACS Catalysis

Research Article

pubs.acs.org/acscatalysis

# A Mn Bipyrimidine Catalyst Predicted To Reduce $CO_2$ at Lower Overpotential

Yan Choi Lam,[†] Robert J. Nielsen,*[,‡] Harry B. Gray,[§] and William A. Goddard, III[†,‡]

[†]Materials and Process Simulation Center, [‡]Joint Center for Artificial Photosynthesis, and [§]Beckman Institute, California Institute of Technology, Pasadena, California 91125, United States

Supporting Information

**ABSTRACT:** Experimentally, $[(L)Mn(CO)_3]^-$ (where L = bis-alkyl-substituted bipyridine) has been observed to catalyze the electrochemical reduction of $CO_2$ to CO in the presence of trifluoroethanol (TFEH). Here we report the atomistic level mechanism of complete catalytic cycles for this reaction, on the basis of DFT calculations (B3LYP-D3 with continuum solvation) of the free energies of reaction and activation, as well as reduction potentials for all catalytically relevant elementary steps. The highly exergonic homoconjugation and carbonation of $TFE^-$ play critical roles in reaction thermodynamics and kinetics, the overall half-reaction being $3CO_2 + 2TFEH + 2e^- \rightarrow CO + H_2O + 2[F_3CCH_2OCO_2]^-$ (calculated standard reduction potential: −1.49 V vs SCE). In the catalytic cycle for CO formation, $CO_2$ coordinates to $[(L)Mn(CO)_3]^-$ (**1a**, L = bpy), and the adduct is then protonated to form $[(L)Mn(CO)_3(CO_2H)]$ (**3a**). **3a** subsequently reacts to form $[(L)Mn(CO)_4]^0$ (**5a**) via one of two pathways: (a) TFEH-mediated dehydroxylation to $[(L)Mn(CO)_4]^+$ (**4a**), followed by one-electron reduction to **5a**, or (b) under more reducing potentials, one-electron reduction to $[(L)Mn(CO)_3(CO_2H)]^-$ (**3′a**), followed by dehydroxylation to **5a**. Pathway b has a lower activation energy by 2.2 kcal $mol^{-1}$. Consequently, the maximum catalytic turnover frequency ($TOF_{max}$) is achieved at ∼−1.75 V vs SCE (∼0.25 V overpotential). For the analogous bipyrimidine compound (not yet studied experimentally), reduction of **3b** to **3′b** occurs at a potential 0.5 V more positive than that of **3a**, and the overpotential required to achieve $TOF_{max}$ is predicted to be lower by ∼0.25 V. This improvement is, however, achieved at the price of a lower $TOF_{max}$, and we predict that **1b** has superior TOF at potentials above ∼−1.6 V vs SCE. In addition, the various factors contributing to product selectivity (CO over $H_2$) are discussed.

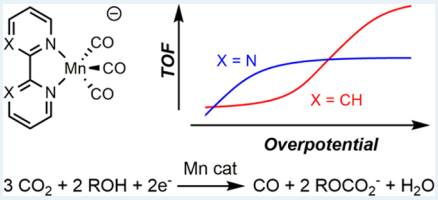


**KEYWORDS:** *density functional theory, electrochemical $CO_2$ reduction, reaction mechanism, chemoselectivity, overpotential*

## INTRODUCTION

Carbon monoxide (CO) is a versatile reagent, employed industrially in the synthesis of phosgene,[1] methanol,[2] and acetic acid[3] and in the production of fuels via the Fischer−Tropsch process.[4] A potentially attractive method for CO production is the electrochemical reduction of carbon dioxide, preferably coupled to water oxidation and driven by renewable energy.

Toward this end, an assortment of homogeneous catalysts has been investigated experimentally and theoretically.[5−9] Among these are *fac*-$[Mn(bpy\text{-}R)(CO)_3]^-$ complexes[9e,f,h] (bpy-R = 4,4′- or 2,2′-disubstituted bipyridine; since all complexes discussed henceforth are *fac*, the label will be omitted), produced by two sequential one-electron reductions of the corresponding Mn(I) halides. This catalytic activity is proton-dependent; indeed, unlike the case with the analogous Re complexes, no catalysis is observed in the absence of weak Brønsted acids such as water, methanol, and trifluoroethanol (TFEH).[9e,f] Notably, CO selectivity is quantitative (within experimental uncertainty), even in the presence of >1 M concentration of the aforementioned acids.

Extensive mechanistic investigations, both experimental[9b,d,10,11] and theoretical,[10,12,13] have elucidated plausible mechanisms for proton-dependent $CO_2$ electrochemical reduction to CO catalyzed by $[Re(bpy\text{-}R)(CO)_3]^-$ complexes. In particular, the $[Re(bpy\text{-}R)(CO)_3]^-$ complexes (**1**-Re) display a kinetic preference for $CO_2$ coordination over protonation at Re, forming $[Re(bpy\text{-}R)(CO)_3(CO_2^-)]$ (**2**-Re), which is protonated to $[Re(bpy\text{-}R)(CO)_3(CO_2H)]$ (**3**-Re).[10,13] This complex may then undergo proton-assisted dehydroxylation to $[Re(bpy\text{-}R)(CO)_4]^+$ (**4**-Re), followed by one-electron reduction to $[Re(bpy\text{-}R)(CO)_4]^0$ (**5**-Re). Alternatively, at higher overpotentials, it undergoes one-electron reduction, followed by proton-assisted dehydroxylation to form **5**-Re.[13] The latter pathway affords a lower activation free energy ($\Delta G^{\ddagger}$) for the rate-determining dehydroxylation step. **1**-Re is regenerated by electrochemical reduction accompanied by loss of CO.[13] The overall reaction is first order in $CO_2$ and second order in acid.[10]

Here, we report ab initio density functional theory (DFT) studies, including effects of solvation and potential, of electrochemical $CO_2$ reduction in the presence of TFEH catalyzed by $[(bpy)Mn(CO)_3]^-$ (**1a**), a system that has been studied experimentally. Given the noninnocent role of bpy in these reactions, we simultaneously studied the more electron-

Received: September 18, 2014
Revised: February 12, 2015
Published: February 16, 2015

 © 2015 American Chemical Society 

DOI: 10.1021/cs501963v
ACS Catal. 2015, 5, 2521−2528

**Scheme 1. Proposed Electrocatalytic Cycle**[a]

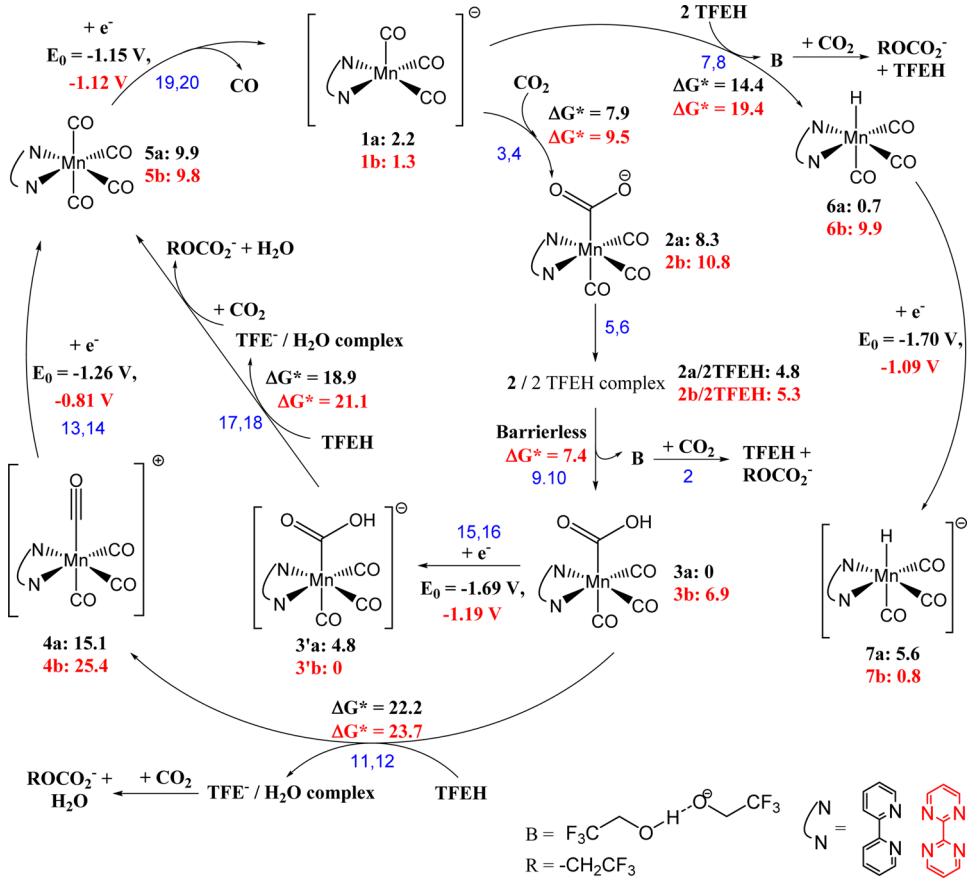


[a]All reagents are in their standard states (25 °C, 1 atm of $CO_2$ and CO, 1 M for all reagents in MeCN). Gibbs free energies (kcal mol$^{-1}$) relative to resting state **3a** (for L = bpy) or **3′b** (for L = bpymd), calculated at −1.49 V vs SCE (0 applied overpotential under standard conditions, see text), are reported in black for L = bpy and in red for L = bpymd. Activation free energies are denoted $\Delta G^*$ and are reported in kcal mol$^{-1}$ relative to the preceding intermediate. Standard reduction potentials are reported in V vs SCE. Numbers in blue refer to entries in Table 1.

deficient bipyrimidine analogue $[(bpymd)Mn(CO)_3]^-$ (**1b**; bpymd = bipyrimidine), which has not yet been studied experimentally. We predict that **1b** produces CO at lower overpotentials than does **1a**.

## COMPUTATIONAL METHODS

Density functional theory (DFT) calculations for geometry optimizations, electronic energy, solvation energy, and vibrational frequencies were performed using the (U)B3LYP hybrid exchange-correlation functional[14] with the D3 dispersion correction,[15] as implemented in the Jaguar software version 7.9.[16] Solvation effects were modeled using the Poisson–Boltzmann continuum (PBF) approximation[17] for acetonitrile ($\varepsilon$ = 37.5, $r$ = 2.18).

Geometry optimizations were performed in the gas phase (for $CO_2$, water, CO, and the TFEH complexes of **2a**,**b**) or acetonitrile (all other species, including transition states) using the 6-311G**++ basis set on organics.[18] For Mn the 1s, 2s, and 2p core electrons were replaced with an ab initio angular momentum projected effective core potential (ECP) of Melius and Goddard[19] using the parameters and 3-$\zeta$ valence functions optimized by Hay and Wadt[20] (LACV3P++) augmented with two $f$ functions.[21]

For the solvation calculations, default van der Waals radii were used during optimization on all atoms, except TFEH, $TFE^-$, the $TFE^-$/TFEH homoconjugate, $F_3CCH_2OCO_2^-$, **2a**, and **2b**, which were optimized with nonstandard van der Waals radii on anionic O atoms (2.0 Å in carboxylates, 2.2 Å in alkoxides) and protic (O-bonded) H atoms (0.75 Å). These radii were chosen because they correctly predicted p$K_a$ values for various neutral organic oxyacids (e.g., phenol) and $\Delta G_{solv}$ values for their conjugate bases (e.g., phenoxide; see the Supporting Information). The free energy of a proton at 1 M in acetonitrile ($G$ = −264.6 kcal/mol) can be obtained from its gas-phase value ($G(H^+, 1\ atm) = H - TS = 2.5k_BT - T \times 26.04$ = −6.3 kcal/mol) plus the empirical solvation energy in acetonitrile ($\Delta G(1\ atm \rightarrow 1\ M, MeCN) = -260.2 + k_BT \ln 24.5$),[22] and this value was used in the benchmarking of p$K_a$ values. However, in the text we have avoided this arbitrary reference state and calculated free energies of reactions involving protons by explicitly considering equilibria among TFEH, $TFE^-$/TFEH homoconjugate, and the carbonate $F_3CCH_2OCO_2^-$ (vide infra). Finally, single-point energy calculations including solvation with these nonstandard van der Waals radii were performed.

Vibrational frequencies were obtained with the same basis sets but without $f$ functions (LACV3P++ for Mn). (As an example, for $[(bpy)Mn(CO)_3]^-$ the largest difference in a normal-mode frequency between calculations at the optimized geometry with and without the $f$ functions was 5 cm$^{-1}$.) All optimized ground-state structures had no imaginary frequency. Most optimized transition state structures had one imaginary



DOI: 10.1021/cs501963v
ACS Catal. 2015, 5, 2521−2528

Table 1. $\Delta G$, $\Delta G^{\ddagger}$, and Standard Reduction Potentials for Reactions in Scheme 1 (R = $F_3CCH_2$)

| | | $\Delta G^a$ | $\Delta G^{\ddagger a}$ | $E^{\circ b}$ |
|---|---|---|---|---|
| 1 | TFEH + $TFE^-$ → B | −13.6 | | N/A |
| 2 | $TFE^-$ + $CO_2$ → $ROCO_2^-$ | −14.6 | | N/A |
| 3 | **1a** + $CO_2$ → **2a** | 6.2 | 7.9 | N/A |
| 4 | **1b** + $CO_2$ → **2b** | 9.5[c] | 9.5[c] | N/A |
| 5 | **2a** + 2 TFEH → **2a**/2 TFEH complex | −3.6 | | N/A |
| 6 | **2b** + 2 TFEH → **2b**/2 TFEH complex | −5.5 | | N/A |
| 7 | **1a** + 2 TFEH → **6a** + B[d] | −0.5 | 14.4 | N/A |
| 8 | **1b** + 2 TFEH → **6b** + B[d] | 1.8 | 19.4 | N/A |
| 9 | **2a**/2 TFEH complex → **3a** + B[d] | −3.8[e] | 0[f] | N/A |
| 10 | **2b**/2 TFEH complex → **3b** + B[d] | 2.6[e] | 7.4 | N/A |
| 11 | **3a** + TFEH → **4a** + $TFE^-/H_2O$ complex[g] | 18.1 | 22.2 | N/A |
| 12 | **3b** + TFEH → **4b** + $TFE^-/H_2O$ complex[g] | 21.6 | 23.7 | N/A |
| 13 | **4a** + $e^-$ → **5a** | N/A | | −1.26 |
| 14 | **4b** + $e^-$ → **5b** | N/A | | −0.81 |
| 15 | **3a** + $e^-$ → **3′a** | N/A | | −1.69 |
| 16 | **3b** + $e^-$ → **3′b** | N/A | | −1.19 |
| 17 | **3′a** + TFEH → **5a** + $TFE^-/H_2O$ complex[g] | 8.1 | 18.9 | N/A |
| 18 | **3′b** + TFEH → **5b** + $TFE^-/H_2O$ complex[g] | 12.8 | 21.1 | N/A |
| 19 | **5a** + $e^-$ → **1a** + CO | N/A | | −1.09 |
| 20 | **5b** + $e^-$ → **1b** + CO | N/A | | −1.12 |
| 21 | $3CO_2$ + 2TFEH + $2e^-$ → CO + $H_2O$ + $2[F_3CCH_2OCO_2]^-$ | N/A | | −1.49 |
| 22 | B + $CO_2$ → $[F_3CCH_2OCO_2]^-$ + TFEH | −1.0 | 2.5 | N/A |

[a]In kcal $mol^{-1}$. [b]In V vs SCE. [c]The reverse reaction appears to be barrierless on the free energy surface because the transition state has a lower zero-point energy (ZPE) than **2b**, offsetting the higher potential energy of the former. [d]Homoconjugate of TFEH and $TFE^-$. [e]This is an upper bound because $TFE^-$/TFEH homoconjugate (B) hydrogen bonds exergonically to **3**, lowering the energy of the products; when B reacts with $CO_2$ to form $[F_3CCH_2OCO_2]^-$, this hydrogen bonding is greatly weakened. [f]The transition state's lower ZPE offsets its higher potential energy. [g]The same transformation can be performed via a transition state involving two TFEH molecules; the $\Delta G^{\ddagger}$ is not, within the uncertainty of the method, significantly different. See text for explanation.

frequency; a few had an additional weak (between 30*i* and 0 $cm^{-1}$) imaginary frequency arising from the rotation of loosely bound solvent molecules. For example, the TS for dehydroxylation of **3a** to **4a** containing two TFEH molecules (see Table 1, entry 11 and footnote *g*) had two imaginary frequencies, one at 496*i* $cm^{-1}$ associated with the reaction coordinate and another at 17*i* $cm^{-1}$ arising from the rotation of a loosely associated TFEH molecule.

Thermodynamic parameters were calculated using the harmonic oscillator, ideal gas, and rigid rotor approximations;[23] in computations of vibrational entropies, all vibrations <50 $cm^{-1}$ not associated with the reaction coordinate of a transition state were replaced with 50 $cm^{-1}$ to avoid spurious fluctuations in entropy arising from low-frequency modes. Standard reduction potentials are reported versus the standard calomel electrode (SCE; absolute potential −4.42 V).[24]

We performed key calculations with a variety of methods regarding solvation, basis set, and functional. As seen in Table S4 in the Supporting Information, neither the replacement of B3LYP-D3 with M06 nor the exclusion of solvation during geometry optimization makes an important difference in reaction free energies or standard reduction potentials in our catalytic cycle. Replacement of B3LYP-D3 with M06 raised reduction potentials by 80−120 mV, while changes in solvation or basis set made smaller differences. The absolute barriers of the rate-limiting dehydroxylation reactions were sensitive to the functional and the atomic radii used in the continuum solvation calculations. Replacing B3LYP-D3 with M06, or employing the alternative atomic radii used throughout the paper, raised the dehydroxylation barriers several kilocalories per mole. However, the difference between these barriers ($\Delta G^{\ddagger}$ in entries 11 and 17, Table 1) underpinning the competition between two reaction pathways remains positive and is only quantitatively altered. Our basic mechanistic conclusions (vide infra) are therefore robust to the choice of computational method.

## RESULTS AND DISCUSSION

Scheme 1 outlines proposed reaction mechanisms for **1** (**1a**,**b**), similar to what Keith et al. proposed for $[(bpy)Re(CO)_3]^-$.[13] TFEH was chosen as the acid in these studies because it afforded the highest TOF among the acids reported.[9f,h] (We have not considered the activation of precatalysts $[(bpy)Mn(CO)_3X]$ and $[(bpymd)Mn(CO)_3X]$, since **1a** and **4a** are isolable solids.) We have not considered the previously reported dimerization of $(L)Mn^0(CO)_3$,[9e,f] because the substitution of sufficiently bulky 6,6′-substituents precludes this reaction.[9h] Thermodynamic and kinetic parameters for all reactions are presented in Table 1, along with standard reduction potentials for reagents and reaction intermediates.

The use of TFEH as an acid leads to the formation of trifluoroethoxide ($TFE^-$), which we expect to be poorly solvated by acetonitrile. The alkoxide can homoconjugate to TFEH (Table 1, entry 1) or react with $CO_2$ to form $[F_3CCH_2OCO_2]^-$ (Table 1, entry 2); both reactions are predicted to be highly exergonic. In computing proton transfer and dehydroxylation transition states, models including either one or two TFEH molecules as the proton source were considered. In the latter models, one TFEH molecule transfers its proton to the Mn complex while the other stabilizes the incipient $TFE^-$ through hydrogen bonding. This stabilization reduces activation enthalpy at the expense of decreased activation entropy. In computing reaction thermodynamics,


DOI: 10.1021/cs501963v
ACS Catal. 2015, 5, 2521−2528

the carbonation reaction must be considered, since it is slightly more exergonic than homoconjugation (see Scheme 1 and Table 1). The above consideration gives rise to an effective calculated p$K_a$ for the combination of TFEH and $CO_2$ (25.1) which is lower than that calculated for TFEH alone (35.8 at infinite dilution: i.e., neglecting homoconjugation of $TFE^-$).[25] The carbonation of the $TFE^-$/TFEH homoconjugate (Table 1, entry 22) is faster than almost any step in the catalytic cycle. The overall half-reaction (Table 1, entry 21) has a calculated reduction potential of −1.49 V vs SCE.

The agreement between calculated and experimentally derived quantities is generally quite good. In particular, the computed potential for the reduction of **3a** (−1.69 V vs SCE) is in good accord with the potential corresponding to $i_{cat} = i_{cat,max}/2$ in the linear scan voltammograms of both Mn(bpy-*t*Bu)$(CO)_3$Br (∼−1.7 V)[9f] and [Mn(mesbpy)$(CO)_3$(MeCN)](OTf) (∼−1.7 V).[9h] The agreement between the calculated $\Delta G^{‡}$ (18.9 kcal $mol^{-1}$ for L = bpy) and the measured TOF (3000 and 5000 $s^{-1}$, respectively, for Mn(bpy-*t*Bu)$(CO)_3$Br and [Mn(mesbpy)$(CO)_3$(MeCN)](OTf), corresponding approximately to $\Delta G^{‡}$ = 16 kcal $mol^{-1}$) is acceptable.

**Coordination of $CO_2$ to Anion 1 and Protonation of the Adduct To Form 3.** At applied potentials typical of controlled-potential electrolysis (CPE) experiments, anion **1** is the resting state in the absence of $CO_2$ and TFEH.[9e,f,h] $CO_2$ coordination to **1** (Table 1, entries 3 and 4) is endergonic but kinetically facile—the reverse reaction is almost barrierless—due to a very early transition state (Mn−C = 2.92 Å for **1a** and 2.86 Å for **1b**; see the Supporting Information for coordinates). (The $CO_2$ adduct **2b** is so shallow a minimum on the potential energy surface that it is unstable at finite temperatures.) The predicted lack of reactivity between **1a** and $CO_2$ is in accord with experimental observations.[9h] In contrast, $CO_2$ coordination was found to be exergonic but rate limiting in a recent Co-based $CO_2$ hydrogenation catalyst.[26]

The $CO_2$ adduct **2** is stabilized by hydrogen bonding to two TFEH molecules (Table 1, entries 5 and 6). Such hydrogen bonding also facilitates proton transfer to form **3** (Table 1, entries 9 and 10) by stabilizing the transition state vis-à-vis $CO_2$ adduct **2**. The rapid and exergonic carbonation of the $TFE^-$/TFEH homoconjugate (Table 1, entry 22) provides an additional driving force for this transformation, rendering the net transformation of **1a** to **3a** mildly exergonic ($\Delta G$ = −2.2 kcal/mol, $K_{eq}$ = 41). This is in agreement with experimental observation, for which the equilibrium constant (L = Mesbpy) is ca. 46 $M^{-1}$ ($\Delta G \approx$ −2.3 kcal $mol^{-1}$) when MeOH is the proton source.[9h]

**Two Pathways for Dehydroxylation of 3: Dominant Mechanism Depends on Applied Potential.** Hydroxycarbonyl complexes **3** and **3′** are converted to tetracarbonyl compounds **4** and **5** via protonolysis of the C−OH bond by the acid TFEH. In the TOF-determining transition states $TS_{3\to4}$ and $TS_{3'\to5}$, $OH^-$ is almost fully dissociated, stabilized by strong hydrogen bonding to TFEH (Figure 1). $TS_{3'\to5}$ has one electron more than $TS_{3\to4}$, resulting in an earlier transition state with significantly shorter C28−O48 (the C−O bond being cleaved) and longer O48−H32 (hydrogen bonding) distances (Figure 1) and reduced activation energies (by 3.3 and 2.6 kcal $mol^{-1}$ for L = bpy and bpymd, respectively). This reduction in activation energy is attributable to the weaker C−OH bond in **3′** vis-à-vis **3** (by 10.0 and 8.7 kcal $mol^{-1}$, respectively, for L = bpy and bpymd; cf. Table 1, entries 11/12 vs entries 17/18).

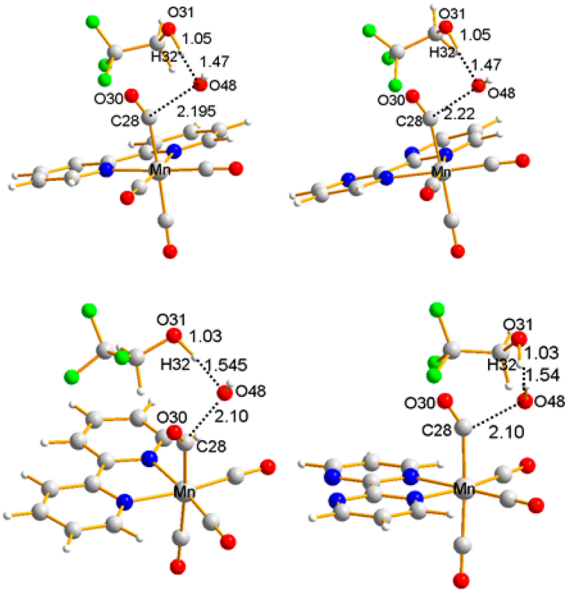


**Figure 1.** Optimized transition states for (top left, $TS_{3a\to4a}$) **3a** + TFEH → **4a** + $TFE^-/H_2O$ complex, (top right, $TS_{3b\to4b}$) **3b** + TFEH → **4b** + $TFE^-/H_2O$ complex, (bottom left, $TS_{3'a\to5a}$) **3′a** + TFEH → **5a** + $TFE^-/H_2O$ complex, and (bottom right, $TS_{3'b\to5b}$) **3′b** + TFEH → **5b** + $TFE^-/H_2O$ complex. All interatomic distances are reported in Å.

Assuming that charge transfer and mass transport are not rate-limiting, **4**, **5**, **1**, **2**, **2**/2 TFEH complex, **3**, and **3′** interconvert on a faster time scale than dehydroxylation of **3** or **3′**. The equilibrium among **1**, **2**, **2**/2 TFEH complex, and **3** is independent of applied potential, with **3a** and **1b** being dominant among these for L = bpy and bpymd, respectively. The equilibrium among **4**, **5**, **3**, and **3′** is potential dependent. For L = bpy, **3a** is the resting state at high applied potentials (low overpotentials); at potentials below $E_{3a/3'a}$ (the reduction potential of **3a**), **3′a** becomes the resting state (Figure 2, top—note that the applied potential decreases and the overpotential increases to the right of the figure). For L = bpymd, the resting state shifts from **1b** to **3′b** below −1.43 V at the assumed standard states (Figure 2, top) because $E_{3b/3'b}$ is −1.19 V (entry 16, Table 1). The dehydroxylation reactions **3** + TFEH → **4** + $TFE^-\cdots H_2O$ (Table 1, entries 11/12) yield particularly endothermic products (e.g., $K_{eq} = 5 \times 10^{-14}$ for **3a** ⇆ **4a** were these allowed to equilibrate). Catalysis via this path relies on the products of this reaction being intercepted by exergonic reactions with low barriers: reduction of **4** and carbonation or homoconjugation of the $TFE^-\cdots H_2O$ complex. Dehydroxylation reactions of **3′** (Table 1, entries 17/18) are less endergonic. As a result of these potential-dependent equilibria, for L = bpy, the flux through rate-determining dehydroxylation reactions **3a** → **4a** or **3′a** → **5a** is also a function of applied potential (Figure 2, bottom). In the potential regime where **3a** is the resting state, total TOF remains constant until **3′a** is formed in significant concentrations. The **3′a** → **5a** pathway begins to dominate at applied potentials higher than $E_{3a/3'a}$ because it has a lower barrier than **3a** → **4a**, and the total TOF increases until **3′a** becomes the resting state (Figure 2, bottom). For L = bpymd, the **3′b** → **5b** pathway dominates at all potentials below −1.33 V.

**Comparison of 1a and 1b as Catalysts for Electrochemical $CO_2$ Reduction.** The bipyrimidine complexes are


DOI: 10.1021/cs501963v
*ACS Catal.* 2015, 5, 2521−2528

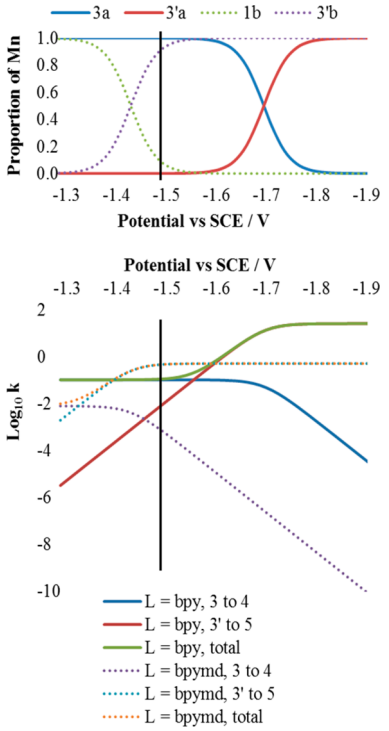


**Figure 2.** (top) Concentration of species **3a** and **3′a** (for L = bpy) or **1b** and **3′b** (for L = bpymd) as a proportion of total Mn concentration. (bottom) Rates for **3** → **4**, **3′** → **5**, and the complete catalytic cycle, as a function of applied potential (vs SCE), for L = bpy (solid lines) and L = bpymd (dotted lines). The computed standard thermodynamic reduction potential (−1.49 V) is marked with a vertical black line.

more easily reduced than their bipyridine analogues because bipyrimidine is more electron deficient and hence a better electron acceptor—reduction potentials of **3b** and **4b** are higher by 0.51 and 0.50 V, respectively, than those of **3a** and **4a** (Scheme 1). The SOMOs of **3′a** and **3′b** (as well as those of tetracarbonyl intermediates **5a** and **5b**) are ligand-based (Figure 3). The more facile reduction of bipyrimidine leads directly to a higher reduction potential for **3b** vis-à-vis **3a**.

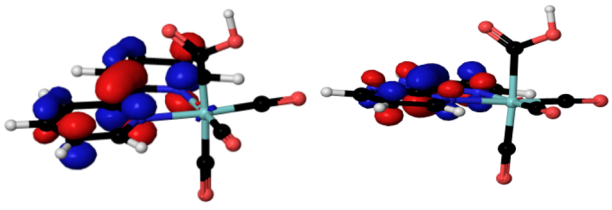

**Figure 3.** Calculated orbital surfaces of the SOMOs in (left) **3′a** and (right) **3′b**.

The dehydroxylation reactions of **3b** and **3′b** have slightly higher $\Delta G^{\ddagger}$ values (by 1.5 and 2.2 kcal mol$^{-1}$, respectively) in comparison to those of **3a** and **3′a**, reflecting slightly stronger (by 3.4 and 4.7 kcal mol$^{-1}$, respectively) C−OH bonds in the bipyrimidine complexes. Since the dissociation of hydroxide involves a net loss of charge from complexes **3** and **3′**, the activation barrier is lower in the case of the less electronegative ligand bpy. The magnitude of this difference is small in comparison to the difference in reduction potentials.

The cumulative effect of these two differences is that whether catalyst **1a** or **1b** affords higher TOFs depends on the applied potential (Figure 2). At potentials above ∼−1.6 V, **1b** provides higher TOFs, because **1b** and **3b** proceed exergonically to **3′b**, accessing the faster dehydroxylation pathway from **3′b** to **5b**. However, when $E$ < −1.6 V, **3a** begins to undergo reduction to **3′a**, and the lower (by 2.2 kcal mol$^{-1}$) activation energy for **3′a** dehydroxylation gives **1a** higher TOFs.

In summary, our calculations show that catalyst **1a** affords a higher maximum TOF ($TOF_{max}$), but at the price of a moderate overpotential (∼0.25 V, −1.75 V vs SCE) to achieve $TOF_{max}$, in line with experimental results showing that $i_{cat}$ for TFEH-mediated $CO_2$ reduction by Mn(bpy-*t*Bu)(CO)$_3$Br peaks at ∼−1.80 V vs SCE.[9e,f] In contrast, catalyst **1b** is predicted to reach $TOF_{max}$ at −1.5 V vs SCE (nominally zero overpotential under standard conditions), albeit at the expense of a lower maximum $TOF_{max}$. (The turn-on potential is lower than the reduction potential of **3b**, reflecting the change in catalyst resting state from **1b** to **3′b**.) Note that the computed *standard* reduction potential of −1.49 V vs SCE assumes the concentrations of $H_2O$ and $[F_3CCH_2OCO_2]^-$ to be 1 M and the pressure of CO to be 1 atm. Under reaction conditions of a cyclic voltammetry (CV) experiment, these concentrations would be lower and the thermodynamic potential concomitantly higher.[27]

**Electronic Structure of 1.** The open-shell singlets of **1a** and **1b** are lower in energy than their corresponding closed-shell singlets by 0.2 kcal mol$^{-1}$,[28] well within the uncertainty of the method. The HOMOs in the closed-shell singlets are delocalized over the metal center and the ligand. In the open-shell singlets, the $\alpha$-HOMOs are predominantly Mn-centered while the $\beta$-HOMOs are delocalized over the noninnocent ligand (bpy or bpymd; Figure 4). For comparison, IR, XANES, and EXAFS data, as well as DFT calculations, indicate a diamagnetic diradical singlet, Re$^0$(bpy)$^-$ ground state for [(bpy-R)Re(CO)$_3$]$^-$.[10b,13]

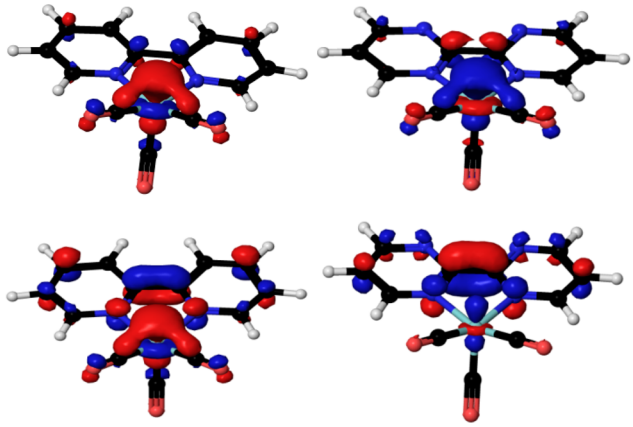

**Figure 4.** (top) $\alpha$-HOMOs and (bottom) $\beta$-HOMOs of (left) **1a** and (right) **1b**.

**Kinetic Selectivity for CO Production.** Assuming protonation at Mn of **1** (to **6**) is the rate-determining step in the production of side products (i.e., $H_2$), and when the steady-state approximation is applied, the selectivity ratio $S$ (the rate of CO formation, $k_{CO}$, divided by that of other products, $k_{other}$) for L = bpy, at potentials where dehydroxylation of **3′a** dominates over that of **3a** (vide supra), is given by[29]


DOI: 10.1021/cs501963v
*ACS Catal.* 2015, 5, 2521−2528

$$S_{\text{low-}\eta} = \left[\frac{k_{1\to3}[CO_2]}{k_{1\to6}[TFEH]^2}\right]\frac{k_{3'\to5}K_{3/3'}[TFEH]}{k_{3\to1}\frac{[F_3CCH_2OCO_2^-]}{[TFEH][CO_2]}} = \left[\frac{k_{1\to3}k_{3'\to5}K_{3/3'}}{k_{1\to6}k_{3\to1}}\right]\frac{[CO_2]^2}{[F_3CCH_2OCO_2^-]} \quad (1a)$$

where L = bpy, $k_{i\to j}$ denotes the rate constant for conversion of species $i$ to $j$, and $K_{3/3'} = \exp[((11600/T)(-1.69 - E))]$ is the equilibrium constant for reduction of **3** to **3′**. Equation 1a applies in the low-overpotential regime, defined by $k_{3'\to5}K_{3/3'}[TFEH] \ll k_{3\to1}([F_3CCH_2OCO_2^-]/[TFEH][CO_2])$. In the high-$\eta$ regime

$$S_{\text{high-}\eta} = \frac{k_{1\to3}}{k_{1\to6}}\frac{[CO_2]}{[TFEH]^2} \quad (1a')$$

where L = bpy.

Equations 1a and 1a′ follow from the predictions that (1) the rate-determining TS for conversion from **1a** to **3a** (and vice versa) is the $CO_2$ addition transition state $TS_{1a\to2a}$ (Scheme 2)

**Scheme 2. Mechanistic Summary Showing Free Energies of Catalytic Intermediates and Transition States Shown in Scheme 1, at $E = E^\circ_{3/3'} - 0.1$ V (−1.79 V vs SCE) for L = bpy (Blue Line) and at $\eta = 0.1$ V (−1.59 V vs SCE) for L = bpymd (Red Line)[a]**

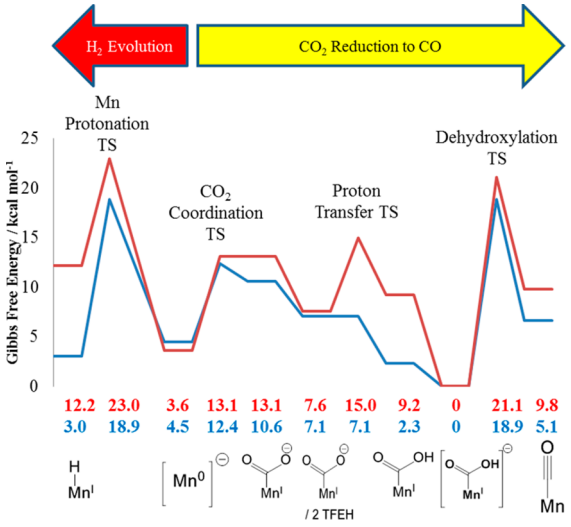


[a]These potentials approximate the minimum overpotential needed to achieve $TOF_{max}$.

and (2) under operating conditions, dehydroxylation of **3′a** is TOF-limiting for CO production. In the high-$\eta$ regime, the dehydroxylation of **3′a** is much faster than its conversion back to **1a**, rendering the conversion of **1a** to **3′a** irreversible. Selectivity is simply the branching ratio between conversion of **1a** to **3a** (and subsequent reduction to **3′a**) and protonation to **6a**. In the low-$\eta$ regime, in contrast, a potential-dependent equilibrium between **1a** and **3′a** precedes TOF- and selectivity-determining dehydroxylation of **3′**.

For the bipyrimidine complex, the rate-determining TS for conversion from **1** to **3** (and vice versa) is the proton transfer transition state $TS_{2b/2TFEH\to3b}$ (Scheme 2). Under the same assumptions as for the bipyridine analogue, in the low-$\eta$ regime defined by $k_{3'\to5}K_{3/3'}[CO_2] \ll k_{3\to1}[F_3CCH_2OCO_2^-]$:

$$S_{\text{low-}\eta} = \left[\frac{k_{1\to3}k_{3'\to5}K_{3/73'}}{k_{1\to6}k_{3\to1}}\right]\frac{[CO_2]^2}{[F_3CCH_2OCO_2^-]} \quad (2a)$$

where L = bpymd and $K_{3/3'} = \exp[((11600/T)(-1.19 - E))]$.

In the high-$\eta$ regime

$$S_{\text{high-}\eta} = \left[\frac{k_{1\to3}}{k_{1\to6}}\right][CO_2] \quad (2a')$$

where L = bpymd.

At 1 M TFEH, the high-$\eta$ regime is approached at a lower (by 0.23 V) overpotential for catalyst **1b** in comparison to that for its bipyridine analogue **1a**. However, since $TOF_{max}$ for **1b** is attained at $\eta < 0.2$ V, operational conditions may more closely approximate the low-$\eta$ regime, where increasing overpotential increases CO selectivity.

Notwithstanding that the activation energy of dehydroxylation (**3′** → **5**) is higher than that of protonation at Mn (**1** → **6**), a combination of factors allows CO to be produced selectively.

(1) *All* steps between **1** and **3′** are faster than protonation of **1**: (a) the endergonic equilibration between **1** and its $CO_2$ adduct **2** is rapid—the loss of $CO_2$ from adduct **2** is essentially barrierless (Table 1, entries 3 and 4)—and (b) homoconjugation between $TFE^-$ and TFEH facilitates proton transfer from TFEH to **2** to form **3** (Table 1, entries 9 and 10).

(2) **3′**, an intermediate in the CO production pathway, is stabilized relative to **1**, a likely hydrogen evolution reaction branching point: (a) the mildly exergonic carbonation of $TFE^-$/TFEH homoconjugate (Table 1, entry 22) improves the thermodynamics of the overall transformation of **1a** to **3a** and (b) under operating conditions, a low potential is applied to maximize TOF, favoring **3′**.

With regard to the rapid equilibration between **1** and its $CO_2$ adduct, Smieja and Benson et al. have proposed that the delocalized electronic configuration of $[(bpy\text{-}R)Re(CO)_3]^-$ favors reaction with $CO_2$ over $H^+$, since the former involves both $\sigma$ and $\pi$ interactions while the latter can only involve $\sigma$ interactions.[10b] If the interaction of filled ligand $\pi^*$ orbitals with $CO_2$ lowers the activation energy for $CO_2$ binding, the orientation of the $CO_2$ fragment with respect to the ligand in $TS_{1\to2}$ (the $CO_2$ addition transition state) should substantially affect such interactions and hence the stability of the TS. Three configurations for $TS_{1a\to2a}$ (Figure 5), in which the N−Mn−C−O dihedral angle was fixed at different values, were optimized. $TS_{1a\to2a''}$ (right), where the $CO_2$ is oriented away from the bpy ligand and has no orbital overlap with the bpy $\pi$ system, was found to have a higher energy (3.7 kcal $mol^{-1}$), suggesting that interaction between bpy-based orbitals and $CO_2$ $\pi^*$ orbitals contributes to kinetic selectivity for $CO_2$ binding

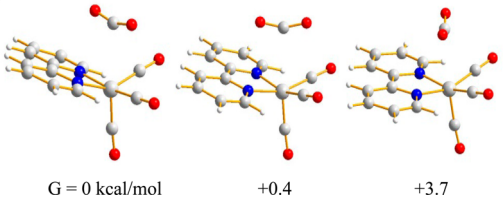


**Figure 5.** Three possible configurations for the **1a** + $CO_2$ → **2a** transition state ($TS_{1a\to2a}$), with N−Mn−C−O dihedral angles fixed at different values: (left) $TS_{1a\to2a'}$, unrestricted; (center) $TS_{1a\to2a''}$, 40°; (right) $TS_{1a\to2a'''}$, −50°.



DOI: 10.1021/cs501963v
ACS Catal. 2015, 5, 2521−2528

and hence CO production. The effect of such $\pi$ overlap on selectivity is significant, despite the long Mn−C distance (>2.9 Å) and $CO_2$−ligand distance (>2.95 Å) in the transition state.

The foregoing discussion suggests that a delocalized electronic structure with redox-active ligands can contribute to selective $CO_2$ reduction to CO. This appears not to be a universal requirement, however. Neither Ni cyclam[7d] nor the phosphine complexes of Pd[8b] have redox-active ligands or delocalized electronic structures. Of equal or greater importance is the maintenance of modest proton activity in the catholyte to suppress metal hydride formation—all of the catalysts referenced here,[6−8a] except the Pd phosphines,[8b] operate in either near-neutral aqueous solutions or polar aprotic solvents with the addition of very weak acids (water, alcohols, and phenol). While formation of the metal−carbon bond during $CO_2$ coordination does not require any bonds to be broken, proton transfer from a weak acid does. In polar aprotic solvents, the highly exergonic homoconjugation and/or carbonation of hydroxide, alkoxides, or phenoxides provides additional driving force for the protonation of $CO_2$ adducts such as **2**, permitting the use of very weak acids which protonate reduced metal centers slowly.

## CONCLUSIONS

We elucidated atomistic reaction mechanisms for Brønsted acid dependent electrochemical $CO_2$ reduction catalyzed by $[(bpy)Mn(CO)_3]^-$ (**1a**). They involve binding of $CO_2$ at the Mn center, followed by proton transfer to form $[(bpy)Mn(CO)_3(CO_2H)]$ (**3a**). Rate-determining dehydroxylation may occur from **3a**, or from once-reduced $[(bpy)Mn(CO)_3(CO_2H)]^-$ (**3′a**), and is dependent on TFEH, the Brønsted acid studied here. Depending on the applied overpotential, either pathway may dominate.

Furthermore, we studied the new compound **1b**, in which bipyridine has been substituted by bipyrimidine. We predict that **1b** catalyzes $CO_2$ reduction by the same mechanism. However, due to the greater electron affinity of bipyrimidine, the reduction of $[(bpymd)Mn(CO)_3(CO_2H)]$ (**3b**) occurs at a potential 0.5 V higher than that of **3a**, so that the maximum TOF of **1b** (albeit somewhat less than that of **1a**) is accessible without the application of potential beyond the standard thermodynamic potential. Tuning the electronic properties of the heterocyclic ligand should permit optimization of catalytic activity, trading activity for overpotential.

Both **1a** and **1b** were found to display kinetic preference for $CO_2$ addition over protonation by TFE. The homoconjugation and carbonation of the conjugate base trifluoroethoxide play key roles in catalyst activity (by driving forward the reaction using an otherwise weak acid) and selectivity (by stabilizing states **3** and **3′** relative to the likely hydrogen evolution reaction branching point **1**). The HOMOs of both **1a** and **1b** are delocalized over the Mn center and the chelating ligand; interaction of $CO_2$ with the ligand appears to play a significant role in stabilizing the $CO_2$ addition transition state.

## ASSOCIATED CONTENT

### Supporting Information

The following file is available free of charge on the ACS Publications website at DOI: 10.1021/cs501963v.

Coordinates and free energy components for all intermediates and transition states and a discussion of the effect of modifying the van der Waals radii used to construct solute cavities on computed $pK_a$ values of oxyacids and $\Delta G_{solv}$ values of their conjugate bases (PDF)

## AUTHOR INFORMATION

### Corresponding Author

*E-mail for R.J.N.: smith@wag.caltech.edu.

### Notes

The authors declare no competing financial interest.

## ACKNOWLEDGMENTS

Y.C.L., who performed the calculations and data analysis, was supported by the National Science Foundation (NSF) through the Centers for Chemical Innovation (CCI), Solar Fuels grant CHE-1305124, as was H.B.G. R.J.N. and W.A.G., who developed the computational strategy, interpretation, and analysis studies, are supported by the Joint Center for Artificial Photosynthesis, a DOE Energy Innovation Hub, supported through the Office of Science of the U.S. Department of Energy under Award Number DE-SC0004993. We gratefully acknowledge Professor Clifford P. Kubiak for helpful discussions.

## REFERENCES

(1) Schneider, W.; Diller, W.; *Ullmann's Encyclopedia of Industrial Chemistry*; Wiley-VCH: Weinheim, Germany, 2005.

(2) Wilhelm, D. J.; Simbeck, D. R.; Karp, A. D.; Dickenson, R. L. *Fuel Process. Technol.* **2001**, *71*, 139−148.

(3) Sunley, G. J.; Watson, D. J. *Catal. Today* **2000**, *58*, 293−307.

(4) Dry, M. E. *Appl. Catal., A* **1996**, *138*, 319−344.

(5) Reviews: (a) Costentin, C.; Robert, M.; Savéant, J.-M. *Chem. Soc. Rev.* **2013**, *42*, 2423−2436. (b) Windle, C. D.; Perutz, R. N. *Coord. Chem. Rev.* **2012**, *256*, 2562−2570. (c) Finn, C.; Schnittger, S.; Yellowlees, L. J.; Love, J. B. *Chem. Commun.* **2012**, *48*, 1392−1399. (d) Benson, E. E.; Kubiak, C. P.; Sathrum, A. J.; Smieja, A. J. *Chem. Soc. Rev.* **2009**, *38*, 89−99.

(6) Fe-porphyrins: (a) Bhugun, I.; Lexa, D.; Savéant, J. M. *J. Phys. Chem.* **1996**, *100*, 19981−19985. (b) Bhugun, I.; Lexa, D.; Savéant, J. M. *J. Am. Chem. Soc.* **1994**, *116*, 5015−5016. (c) Bhugun, I.; Lexa, D.; Savéant, J. M. *J. Am. Chem. Soc.* **1996**, *118*, 1769−1776. (d) Costentin, C.; Drouet, S.; Robert, M.; Savéant, J. M. *Science* **2012**, *338*, 90−94.

(7) Co and Ni heterocycles and macrocycles: (a) Fisher, B. J.; Eisenberg, R. *J. Am. Chem. Soc.* **1980**, *102*, 7361−7363. (b) Lieber, C. M.; Lewis, N. S. *J. Am. Chem. Soc.* **1984**, *106*, 5033−5034. (c) Beley, M.; Collin, J.-P.; Ruppert, R.; Sauvage, J.-P. *J. Chem. Soc., Chem. Commun.* **1984**, 1315−1316. (d) Froehlich, J. D.; Kubiak, C. P. *Inorg. Chem.* **2012**, *51*, 3932−3934. (e) Tinnemans, A. H. A.; Koster, T. P. M.; Thewissen, D. H. M. W.; Mackor, A. *Recl. Trav. Chim. Pays-Bas.* **1984**, *103*, 288−295.

(8) Phosphine complexes: (a) Szymaszek, A.; Pruchnik, F. P. *J. Organomet. Chem.* **1989**, *376*, 133−140. (b) DuBois, M. R.; DuBois, D. L. *Acc. Chem. Res.* **2009**, *42*, 1974−1982.

(9) Complexes with bipyridine and related ligands: (a) Hawecker, J.; Lehn, J.-M.; Ziessel, R. *J. Chem. Soc., Chem. Commun.* **1984**, 328−330. (b) Patrick Sullivan, B.; Bolinger, C. M.; Conrad, D.; Vining, W. J.; Meyer, T. J. *J. Chem. Soc., Chem. Commun.* **1985**, 1414−1416. (c) O'Toole, T. R.; Margerum, L. D.; Westmoreland, T. D.; Vining, W. J.; Murray, R. W.; Meyer, T. J. *J. Chem. Soc., Chem. Commun.* **1985**, 1416−1417. (d) Smieja, J. M.; Kubiak, C. P. *Inorg. Chem.* **2010**, *49*, 9283−9289. (e) Bourrez, M.; Molton, F.; Chardon-Noblat, S.; Deronzier, A. *Angew. Chem., Int. Ed.* **2011**, *50*, 9903−9906. (f) Smieja, J. M.; Sampson, M. D.; Grice, K. A.; Benson, E. E.; Froehlich, J. D.; Kubiak, C. P. *Inorg. Chem.* **2013**, *52*, 2484−2491. (g) Bruce, M. R. M.; Megehee, E.; Sullivan, B. P.; Thorp, H.; O'Toole, T. R.; Downard, A.; Meyer, T. J. *Organometallics* **1988**, *7*, 238−240. (h) Sampson, M. D.; Nguyen, A. D.; Grice, K. A.; Moore, C. E.; Rheingold, A. L.; Kubiak, C.



DOI: 10.1021/cs501963v
*ACS Catal.* 2015, 5, 2521−2528

P. *J. Am. Chem. Soc.* **2014**, *136*, 5460−5471. (i) Zeng, Q.; Tory, J.; Hartl, F. *Organometallics* **2014**, *33*, 5002−5008.
(10) (a) Smieja, J. M.; Benson, E. E.; Kumar, B.; Grice, K. A.; Seu, C. S.; Miller, A. J. M.; Mayer, J. M.; Kubiak, C. P. *Proc. Natl. Acad. Sci. U. S. A.* **2012**, *109*, 15646−15650. (b) Benson, E. E.; Sampson, M. D.; Grice, K. A.; Smieja, J. M.; Froehlich, J. D.; Friebel, D.; Keith, J. A.; Carter, E. A.; Nilsson, A.; Kubiak, C. P. *Angew. Chem., Int. Ed.* **2013**, *52*, 4841−4844. (c) Sampson, M. D.; Froehlich, J. D.; Smieja, J. M.; Benson, E. E.; Sharp, I. D.; Kubiak, C. P. *Energy Environ. Sci.* **2013**, *6*, 3748−3755.
(11) Wong, K.−Y.; Chung, W.-H.; Lau, C.-P. *J. Electroanal. Chem.* **1998**, *453*, 161−169.
(12) Agarwal, J.; Sanders, B. C.; Fujita, E.; Schaefer, H. F.; Harrop, T. C.; Muckerman, J. T. *Chem. Commun.* **2012**, *48*, 6797−6799.
(13) Keith, J. A.; Grice, K. A.; Kubiak, C. P.; Carter, E. A. *J. Am. Chem. Soc.* **2013**, *135*, 15823−15829.
(14) Becke, A. D. *J. Chem. Phys.* **1993**, *98*, 5648−5652.
(15) Grimme, S.; Antony, J.; Ehrlich, S.; Krieg, H. *J. Chem. Phys.* **2010**, *132*, 154104−154119.
(16) *Jaguar*; Schrödinger, LLC: New York, 2012.
(17) Marten, B.; Kim, K.; Cortis, C.; Friesner, R. A.; Murphy, R. B.; Ringnalda, M. N.; Sitko, D.; Honig, B. *J. Phys. Chem.* **1996**, *100*, 11775−11788.
(18) (a) Krishnan, R.; Binkley, J. S.; Seeger, R.; Pople, J. A. *J. Chem. Phys.* **1980**, *72*, 650−654. (b) Clark, T.; Chandrasekhar, J.; Spitznagel, G. W.; Schleyer, P. V. R *J. Comput. Chem.* **1983**, *4*, 294−301.
(19) (a) Melius, C. F.; Goddard, W. A., III *Phys. Rev. A* **1974**, *10*, 1528−1540. (b) Melius, C. F.; Olafson, B. D.; Goddard, W. A., III *Chem. Phys. Lett.* **1974**, *28*, 457−462.
(20) Hay, P. J.; Wadt, W. R. *J. Chem. Phys.* **1985**, *82*, 270−283.
(21) Martin, J. M. L.; Sundermann, A. *J. Chem. Phys.* **2001**, *114*, 3408−3420.
(22) Kelly, C. P.; Cramer, C. J.; Truhlar, D. G. *J. Phys. Chem. B* **2007**, *111*, 408−422.
(23) McQuarrie, D. A. *Statistical Mechanics*; University Science Books: Sausalito, CA, 2000.
(24) Isse, A. A.; Gennaro, A. *J. Phys. Chem. B* **2010**, *114*, 7894−7899. Treating an electron at SCE as a reactant yields an effective free energy (relative to an electron at rest under vacuum, the reference state of QM calculations) of 23.06 (cal/(mol/eV)) × −4.42 (V) × $1e^-$ = −102.0 kcal/mol.
(25) In the context of the hydrogen evolution reaction, Fourmond and co-workers have pointed out the importance of accounting for homoconjugation in determining overpotential. See: Fourmond, V.; Jacques, P.-A.; Fontecave, M.; Artero, V. *Inorg. Chem.* **2010**, *49*, 10338−10347.
(26) Kumar, N.; Camaioni, D. M.; Dupuis, M.; Raugei, S.; Appel, A. M. *Dalton Trans.* **2014**, *43*, 11803−11806.
(27) The product (in our case, CO, $F_3CCH_2OCO_2^-$, and $H_2O$) concentration is typically very low under the conditions of cyclic voltammetric (CV) experiments. The concentration of $F_3CCH_2OCO_2^-$ in bulk electrolysis experiments has not been determined. A reasonable estimate may be deduced using a typical catalyst concentration of 1 mM and TON = 20. In this case, $[F_3CCH_2OCO_2^-]$ is no more than 40 mM (since two molecules are produced for every molecule of CO formed).
(28) Open shell singlet calculations were performed by obtaining the triplet wave function, then changing the $\alpha$ HOMO into a $\beta$ orbital and reoptimizing the wave function and geometry. This resulted in a singlet configuration in which the ligand-based electron is antiferromagnetically coupled to an overlapping Mn-based electron. Closed-shell singlet calculations were performed using the RDFT formalism. Since the DFT-computed energy of the open-shell singlet is an upper bound on the energy of the true (spin-uncontaminated) singlet, the latter is lower in energy than the closed-shell singlet.
(29) Note that, throughout this article, the reference concentration for $CO_2$, $[CO_2]_0$, is 1 atm or ca. 0.28 M in acetonitrile.


DOI: 10.1021/cs501963v
*ACS Catal.* 2015, 5, 2521−2528